Innovative Solar Photovoltaic and Thermoelectric Power Generator for a Recirculating Aquaculture System

Gideon Kidegho*‡, Robert Kinyua**, Christopher Muriithi***, Francis Njoka*

*Institute of Energy and Environmental Technology, Jomo Kenyatta University of Agriculture and Technology, P.O. Box 62000-00200 Nairobi, Kenya.
**Department of Physics, College of Pure and Applied Sciences, Jomo Kenyatta University of Agriculture and Technology, P.O. Box 62000-00200 Nairobi, Kenya.
***Department of Electrical & Electronic Engineering, School of Engineering and Technology, Murang'a University of Technology, P.O. Box 75-10200 Murang'a, Kenya.
(kidegho.gideon@students.jkuat.ac.ke, kinyua@fsc.jkuat.ac.ke, cmmuriithi@mut.ac.ke, fnjoka@ieet.jkuat.ac.ke)

‡Corresponding Author; Gideon Kidegho, P.O. Box 62000-00200 Nairobi Kenya, Tel: +254-721 919113, kidegho.gideon@students.jkuat.ac.ke,

Received: 18.03.2020 Accepted:16.05.2020

Abstract-

Solar Photovoltaic power generation is fast gaining popularity in Kenya. However, the effects of high cell temperatures continue to be a major hindrance to their efficiency especially for standalone systems. Water can be used for cooling when combined with thermoelectric generators (TEG) in areas where it is available achieving double gains. Kisumu Nyalenda, in Kenya is one such site where weather and irradiance data have been collected for the design of a PV+TEG power generation system. In this paper, a 3-tier study is conducted to evaluate TEG power, voltage, current and temperature distribution and the overall performance of the hybrid system. Numerical simulations are conducted on Matlab Simulink platform model based on a medium temperature gradient (10 ^{0}C - 100 ^{0}C) category TEG. Bench study setups are done replicating the weather and irradiation conditions of a Recirculation Aquaculture System (RAS) in Nyalenda Kisumu. The TEG bench results are then used to guide the design of the autonomous PV+TEG power generation system. Obtained results confirm that by accurately modelling the TEG and matching its internal resistance to the load, maximum power can be achieved. It is further confirmed that using series-parallel connection of TEGs stack under PV modules operating at temperature gradients varying between 5 ^{0}C to 35 ^{0}C, a 20 kWp PV system gains an extra 15.7% from TEG array with a further 1.05% power gain from PV module temperature reduction.

Keywords: Thermoelectric generators, Temperature gradient, PV Cooling, Autonomous Aquaculture system

1. Introduction

Solar Photovoltaic (PV) power generation is growing fast world over and is expected to occupy about 30% -50% of electricity generation by 2050 [1]. Unfortunatelty the PV modules heat up as they generate electricity outdoors. When the sun's irradiation spectrum strikes the PV module, the PV cells are only capable of effectively converting a portion of the incident photons into electricity as per the cell's efficiency and band-gap energy requirements. The remaining photons result into heat that ends up heating up the solar cell [2]. In their study, Razak et al showed that PV modules' elevated temperature reduced the output voltage and subsequently its power production [3]. Investigations carried out by Xu et al on ultra-broadband (300 - 2500 nm) photon management for crystalline silicon thin film solar cells using Finite Difference Time Domain proposed a novel thin film cell structure[4]. Currently, the most popular cells are silicon solar cells with efficiency of 24.4 % due to the limitations of the absorbed solar photon energy [5]. The temperature phenomenon is more common in the tropical and sub-tropical regions and greatly affects PV power generation efficiencies and cause degradation like corrosion. This high cell temperature problem can be mitigated through cooling of PV modules. Akbar R.N. et al [6] implementated a TEG cooling in extreme temperatures and observed that TEGs are capable of absorbing the energy of the Alpha, Beta and Gamma particles in addition to the complete electromagnetic spectrum to generate electricity. The objective of this paper is to evaluate the performance of a PV-TEG power generation system intended for a recirculating aquaculture system located in a tropical region which is endowed with large water reserves.

2.0 PV-TEG Cell Performance Improvement Studies

Many studies have been carried out to mitigate PV system power loss due to elevated cell temperatures and improve power generation efficiency in tropical regions. Temaneh, and Mukwekwe showed that a 37.8 kWp solar PV system operating at an average module temperature of 35.4 ^{0}C in Namibia lost at least 3.21% of its rated system power output due to high cell temperatures [7]. This affects the design and sizing of PV systems and in the process, usually resulting in oversized PV systems to avoid shortfalls in the energy harvest [8]. In an experimental and simulation PV cooling system method by Benhmida M. et al [9] resulted in an improvement of electrical efficiency by 0.046%/ ^{0}C and a 48 ^{0}C to 24 ^{0}C temperature decrease.

Many methods have been developed to try and mitigate high PV cell temperatures like; creating adequate cooling air between the module's back plates and the mounting surface, cooling the PV modules using Nano fluids, use of microchannel heat sinks, use of phase change materials (PCM), use of cooling panels and even floating the PV modules on water forms [10–13]. Al Shohani et al, presented investigations of a novel optical water filter (OWF) for PV-thermal (PVT) and concentrated PV-thermal (CPVT) module systems using a water layer of wavelength range of (0.35μm-1μm) and thickness of (1cm - 5cm) and observed that the water layer enhanced the PV performance and also prevented cyclical thermal stresses on the PV cells. They further conducted experiments aimed at reducing heat accumulation in a PV module using OWF and observed that PV module temperatures decreased with increasing thickness of the OWF layer [14]. Elsewhere, Rosa M. et al also investigated use of OWF method on photovoltaic-thermal (PV-T) systems and observed that their implementation resulted in a small reduction in electrical energy, but contributed significantly on thermal energy subsequently increasing the overall system efficiency [15].

The use of Thermoelectric Generators (TEG) to absorb the heat from the hot PV modules and utilizing the absorbed heat to generate electricity is developing into a more suitable method as it enables full utilization of the solar radiation spectrum [16]. Dallan et al demonstrated that TEG modules can absorb the heat from the PV modules and convert it into electricity hence can increase the electricity generation efficiency of the PV + TEG system by up to 3.9% depending on the temperature gradient [17]. Belkaid et al [18] suggested and simulated a new configuration of PV-TEG hybrid standalone generation system and observed that the two technologies complement each other well making possible continuos production and efficiency improvement of the hybrid system . Liu C et al demonstrated that besides generating electricity, TEG modules are noise free, static, environmentally non-polluting, highly reliable and compact in stature [19]. Li G. et al did analysis of the feasibility of PV-TEG looking into the challenges affecting solar systems efficiency [20]. Soltani et al investigated four cooling methods using; natural air, S_iO_2/water, forced air and Fe_3O_4/water cooling. They observed that S_iO_2/water cooling yielded the best efficiency improvement of 3.35% followed by Fe_3O_4/water with 3.13% [21]. Further, Lin J. et al, using a model of PV-TEG hybrid system established the performance, optimal characteristics and optimum operating regions for maximum efficiency and power output [22]. Zhang J. et al also showed that PV-TEG could increase PV cell output by 14% with an added TEG generation of 60% due to improved thermal contact resistance [23]. Abu-Rahmeh T. M., investigated nano-fluids, tap water and aluminium fins and presented a PV cooling method using nano-fluid (0.04%wt TiO_2/water) and obtained higher electricity yield by 5.37% compared to the uncooled PV [24]. Hashim H. et al, developed a model for PV-TEG hybrid system geometry optimisation to achieve increased overall power output and conversion efficiency [25]. Kohei K. et al [26] used varying pitch and interlocking grooves for TEG heat transfer and observed that increasing contact area and pitch of the groove reduced thermal resistance. Solar PV-TEG power generation is gaining popularity as the research and manufacture of Thermoelectric Materials (TEM) of higher figure of merit (Zt) advances [23,27]. Hidaka A. et al [28] examined a TEG coupled with a low voltage boost converter and observed 100% tracking efficiency and effective harvest of thermal energy.

However, aspects like accurate modelling, impedance matching, temperature mismatch and accurate operating weather conditions prediction, have remained a big challenge to effective implementation. Selection of appropriate TEG module type, cooling method and temperature gradient is also of significant importance to the success of these systems.

In this study, considerable efforts are made to match the impendence of the TEG to that of the load and temperature mismatches between the modules mitigated. In addition, modification of local weather conditions and temperature gradient by use of a water body is incorporated in the PV-TEG setup. A medium temperature gradient TEG has been modelled and simulated using both field weather and irradiance parameters from a site in Nyalenda Kisumu and bench setups fabricated using a commercially available TEG to observe their actual behavior.

3.0 Experimental Procedures

In PV-TEG setups, thermal energy recovery is accomplished using TEG modules. These modules are composed of electrically series-connected and thermally parallel-connected P-N junction pairs. Normally in one TEG module, there are practically about 127 P-N junction pairs [29]. When the electrically series-connected P-N junction pairs are subjected to a temperature gradient (ΔT) between the two faces of the modules, they generate electromotive force (EMF) and current flows according to the Seebeck phenomenon [30].

3.1 Numerical Model Setup

For purposes of modelling the TEG module, collected PV module temperature data at the study site are used. The data is obtained from the field setup at Nyalenda Kisumu. With the observed PV cell temperature of 69.2 ^{0}C, a TEG with medium ΔT of 10 ^{0}C - 100 ^{0}C and maximum hot side temperature Th of 150 ^{0}C is selected and its parameters evaluated for simulation purposes. A mathematical model is developed and simulated on a Matlab Simulink platform. In a PV-TEG hybrid power generation system, the thermoelectric generator pellet is both a thermal absorber and an electric generator combining the two functions to achieve electricity generation. Therefore, to be able to accurately model the TEG pellet, all the possible thermal and electrical parameters are considered. The model can be thought of as an electric generator encased in a thermal

vessel consisting of the P and N pellets combination conducting heat in one direction of flow from the hot side, Q_h at temperature, T_h to the cold side, Q_c at temperature, T_c as shown in Fig. 1. The model depicts the contact thermal resistance R_{ct} of the Thermoelectric Material (TEM), the thermal resistance, R_{et} of the P and N elements of the TEG, T_h and Q_h as the temperature and heat respectively, at the hot side of the pellet and T_c and Q_c as the temperature and heat, respectively, at the cold side of the TEG.

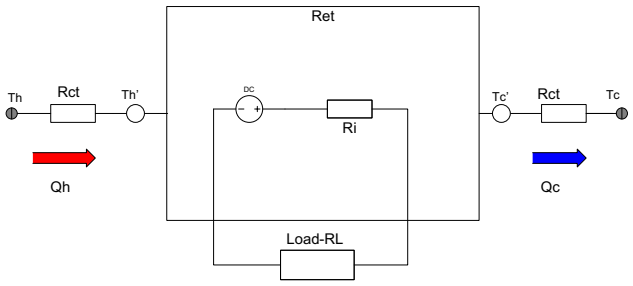

Fig. 1. TEG model block diagram

3.1.1 The Electrical Model of TEG

In the electric model, R_i and R_L are the TEG internal electrical resistance and the load resistance, respectively. The internal electrical resistance of the TEG includes the electrical contact resistance of the associated connecting conductors. During the execution of simulations on the developed model, heat, Q_h is applied on one side of the module that consequently raises the temperature to T_h with conductive heat transfer taking place across to the module to the cold side to appear as Q_c and the temperature as T_c as shown in Fig. 2 T_h and T_c creates a temperature gradient, ΔT that enables the TEG to generate electricity based on the Seebeck phenomenon where the N element assumes the positive polarity and the P element, the negative polarity as shown in Fig.2.

The key internal and external parameters of the TEG pellet used in the model are listed in Tables 1 and 2, respectively.

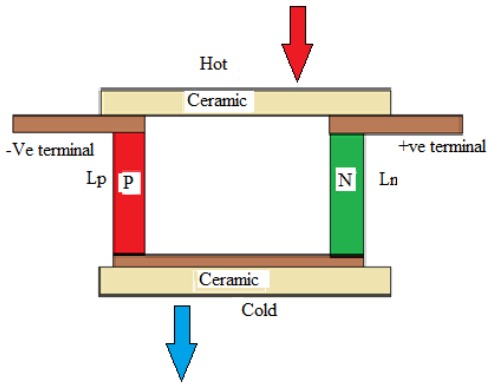

Fig. 2. TEG physical structure

Table 1. Internal parameters of a TEG module

Serial	Parameter description	Symbol
1	Seebeck coefficient for the P element	α_p
2	Seebeck coefficient for the N element	$-\alpha_n$
3	Electrical resistivity for the P element	ρ_{pe}
4	Electrical resistivity for the N element	ρ_{ne}
5	Length of the P element	L_p
6	Length of the N element	L_n
7	Area of the P element	A_p
8	Area of the N element	A_n
9	Thermal resistance of the pellet	R_{th}
10	Terminal resistance of connectors	R_c
11	Number of pellets	N

Table 2. External parameters of a TEG module

Serial	Parameter description	Symbol
1	Temperature gradient	ΔT
2	Hot side temperature	T_h
3	Cold side temperature	T_c
4	Thermal conductivity layer	C_{tl}
5	Load resistance	R_L

The governing equations used in the setting up of the electrical performance model of the TEG are hence developed as follows;

The open circuit voltage or Seebeck voltage for a single pellet of the TEG is given as [31,32];

$$V_{oc} = \alpha \Delta T \quad (1)$$

Where, α is the Seebeck coefficient of the thermoelectric materials (P and N) and ΔT is the temperature gradient between the hot and cold sides of the TEG. For a whole TEG module, the Seebeck coefficient is multiplied by the number of pellets in the module which is typically 127.

The power generated by the TEG or the output power P_o can be expressed as I^2R_L. So, the power output from the TEG for one TEG pellet is given as [19,31];

$$P_o = \alpha I \Delta T - rI^2 \quad (2)$$

Taking the derivative of P_o with respect to current yields

$$\frac{dP_o}{dI} = \alpha \Delta T - 2rI \quad (3)$$

For peak current condition, the derivative is equated to zero ($\alpha \Delta T - 2rI = 0$),

Hence peak current, I_p becomes;

$$I_p = \frac{\alpha \Delta T}{2_r} \quad (4)$$

But I and P_o can, respectively, be expressed as;

$$I = \frac{V}{R} = \frac{\alpha \Delta T}{r + R_L} \quad (5)$$

$$P_o = I^2 R_L = \left(\frac{\alpha \Delta T}{r + R_L}\right)^2 R_L \quad (6)$$

The electrical current flowing in the circuit and across the load R_L is equal to;

$$I_L = \frac{\alpha \Delta T}{r_i + R_L} \quad (7)$$

And can also be given as;

$$I_L = (V_{OC} - r_i I_L)/R_L \quad (8)$$

Therefore, load voltage, V_L is expressed as;

$$V_L = V_{oc} - I_L r_i \quad (9)$$

3.1.2 Thermal Model of the TEG

The thermal model of the TEG pellet is developed based on Fig. 3 and with the understanding that the heat from the heat generator encounters some thermal resistance and the current generated by the TEG also encounters some electrical resistance as it flows through the Thermoelectric Material (TEM), thus creating the Joule heat I^2r in the elements [19,31].

From Fig. 3, the temperature gradient, ΔT is equal to $T_h - T_c$ and the Seebeck coefficient, α shall be equal to $\alpha_p - \alpha_n$ which is the sum of the Seebeck coefficients of the P and N because they are thermally parallel.

The heat applied at the hot side of the TEG is Q_h and the heat dissipated on the cold side is Q_c. Therefore, the heat absorbed by the TEG is given as [33,34];

$$Q_h - Q_c = Q_d \quad (10)$$

Considering a module of n pellets, the thermal power at the hot side can be expressed as [33,34];

$$Q_h = \left(\frac{T_h - T_c}{R_{et}}\right) + T_h n\alpha I - \frac{1}{2} I^2 R_i \quad (11)$$

Where R_{et} is the thermal resistance of the P and N elements, I the electric current flowing in the TEG and, $n\alpha$ is the combined Seebeck coefficients of the P and N elements of the TEG.

Similarly, the thermal power reaching the cold side of the TEG is expressed as [33,34];

$$Q_c = \left(\frac{T_h - T_c}{R_{et}}\right) + \alpha n I T_c + \frac{1}{2} R_i I^2 \quad (12)$$

From Equations (11) and (12), the difference in the value (Q_d) between the hot and the cold side of the TEG is converted to electricity according to the Seebeck phenomenon.

Electrical power, P_o of the TEG is hence equal to the thermal power, Q_d and the efficiency of the TEG can be expressed in both electrical and thermal terms as;

$$\eta = \frac{output\ power}{input\ power} = \frac{P_o}{Q_h} \quad (13)$$

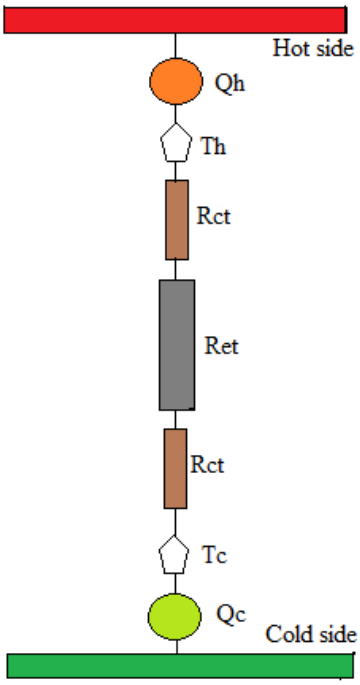

Fig. 3: TEG PN Pellet

3.1.3 Model Development and Simulation

The TEG numerical model is developed using the internal parameters of the TEG pellet obtained from the TEG manufacturers. The parameters values were used in the Matlab Simulink block-sets and built to make the TEG pellet by interconnecting the block-sets using numerical function operators. Display points are used to closely monitor the individual operation outputs and finally the results are obtained from a five-channel oscilloscope that outputs the values in graphical format. For clear visibility of the graticule traces, gains have been used where necessary. The scope output traces consist of the voltage, current, power, efficiency and the TEG hot side temperature, *Th*. The control parameters are the hot side and cold side temperatures of the TEG, *Th and Tc,* respectively. Fig. 4 shows the simulation flowchart for the TEG and Fig. 5 shows the actual numerical operators used in the model.

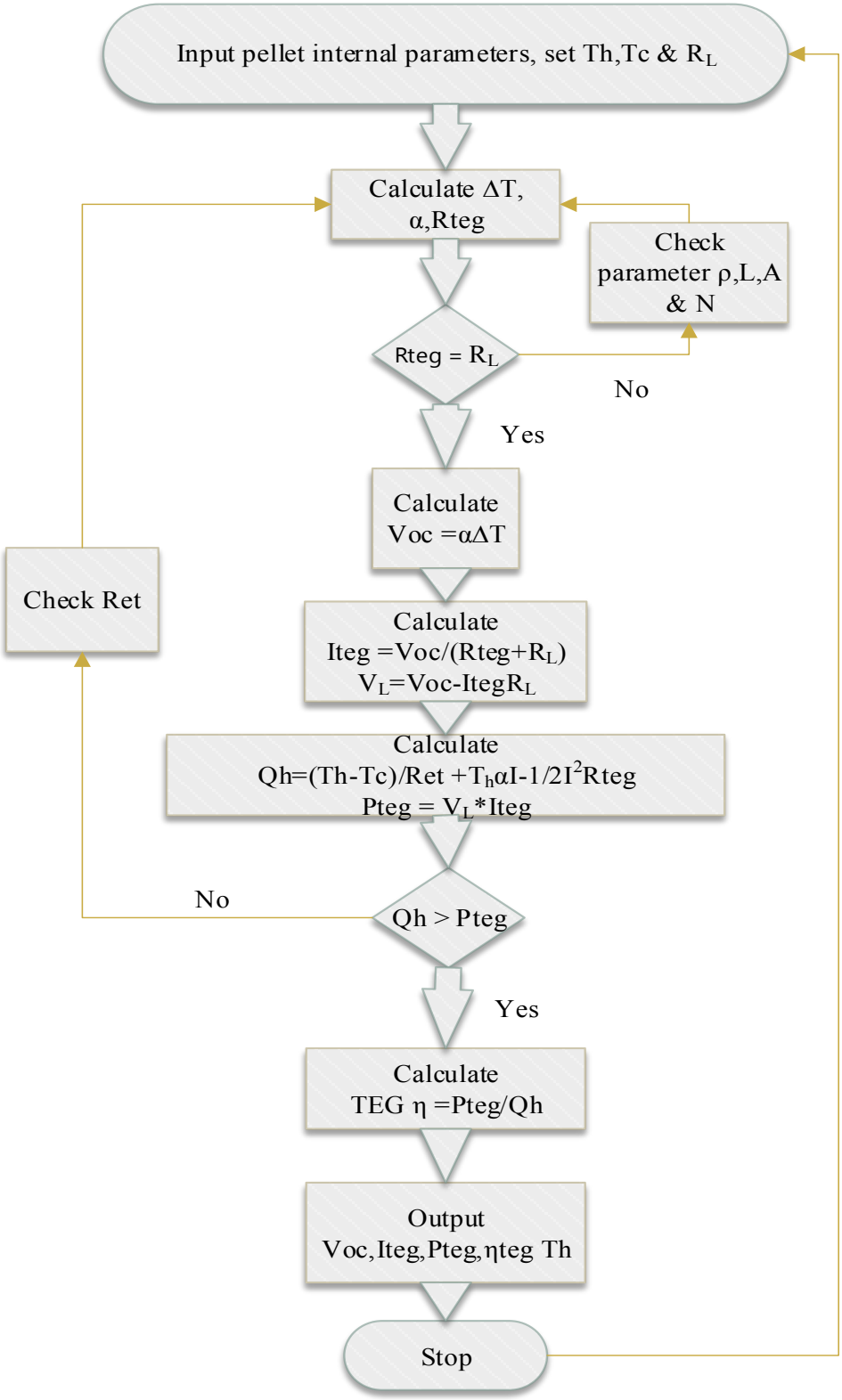

Fig. 4. The TEG simulation state flowchart

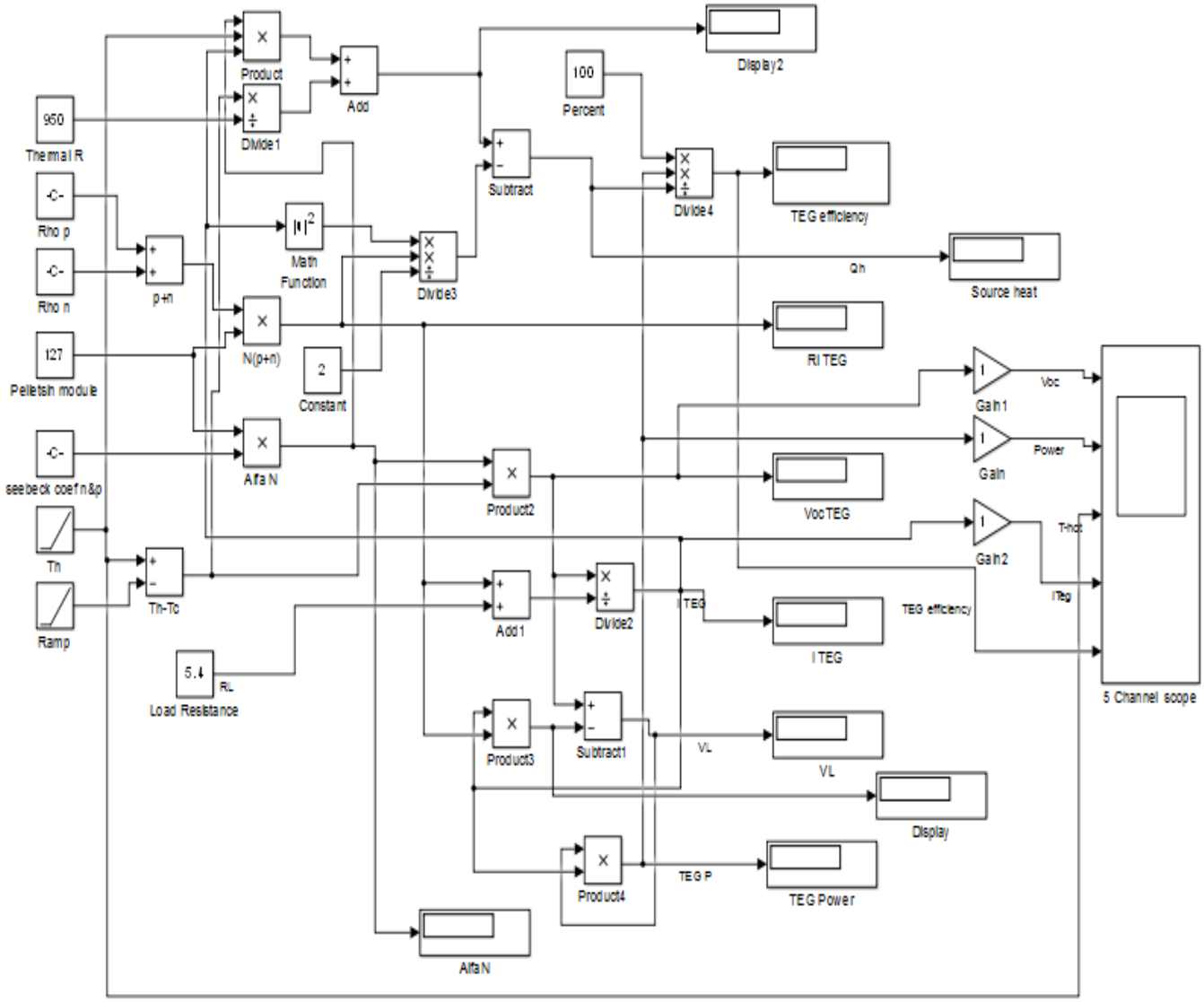

Fig. 5. Schematic TEG model in Matlab Simulink

3.1.4 Model Development Assumptions

During the development of the TEG model, some assumptions were made. The temperature at the back plate of the PV module is taken to be the same as the temperature of the hot side of the TEG implying a near perfect thermal conducting layer between the two surfaces. The internal resistance of the TEG remains constant during the power generation and the temperature of all the pellets is uniform. It is also assumed that the temperature starts from a low value and rises steadily to the maximum field value. The thermal resistances, R_{ct} of the pellets are taken to be insignificant compared to R_{et} in the electrical model of the TEG. Fig. 5 shows a schematic block set of the TEG model used in the Matlab Simulink simulation platform.

3.2 TEG Bench Setup Fabrication

The TEG experimental bench test apparatus are fabricated and set up to carry out measurements of voltage, current and power output from the physical TEG module. The workbench laboratory setups are fabricated for a single, two and four TEG modules. The heat dissipated by the PV is modelled using an electric heater plate and water cooling achieved using an Alucore honey comb cooling panel initially filled with cold water at 20 ^{0}C. Temperatures are measured using K-type thermocouples.

Fig. 6 shows a schematic representation of the electrical connection of a single TEG and position of the thermocouples, while Figs. 7a, 7b and 7c show the single, two and four TEG setups, respectively. Their respective electrical connections are schematically presented in Fig. 8. For each of the setups, the load resistance was matched to the TEG internal resistance as shown. The load current drawn from the TEG modules was measured as a voltage across a 1ohm resistor. The data from these setups is continuously logged using a KEYENCE NR-500 logger at time intervals of 5/10 seconds and the data collected in CSV format using a laptop computer.

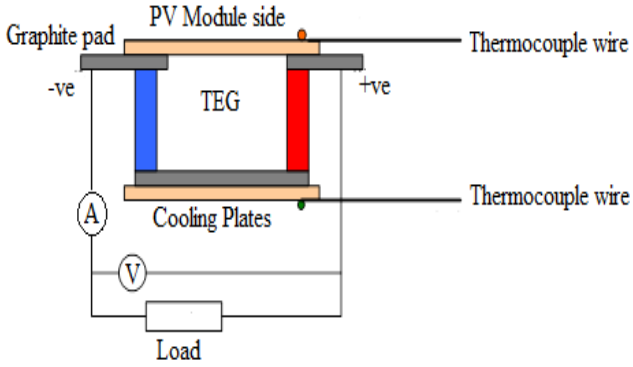

Fig. 6. TEG connection schematic

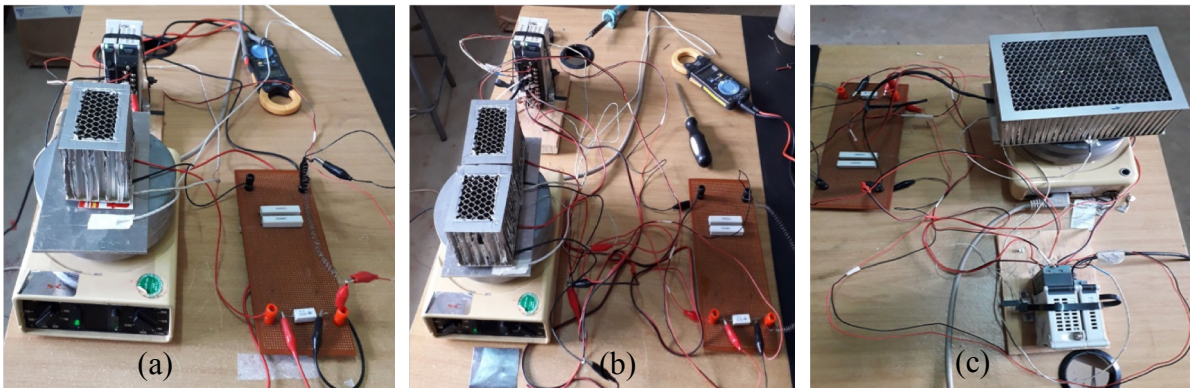

Fig. 7. Laboratory TEG setups; (a) single, (b) two and (c) four TEGs

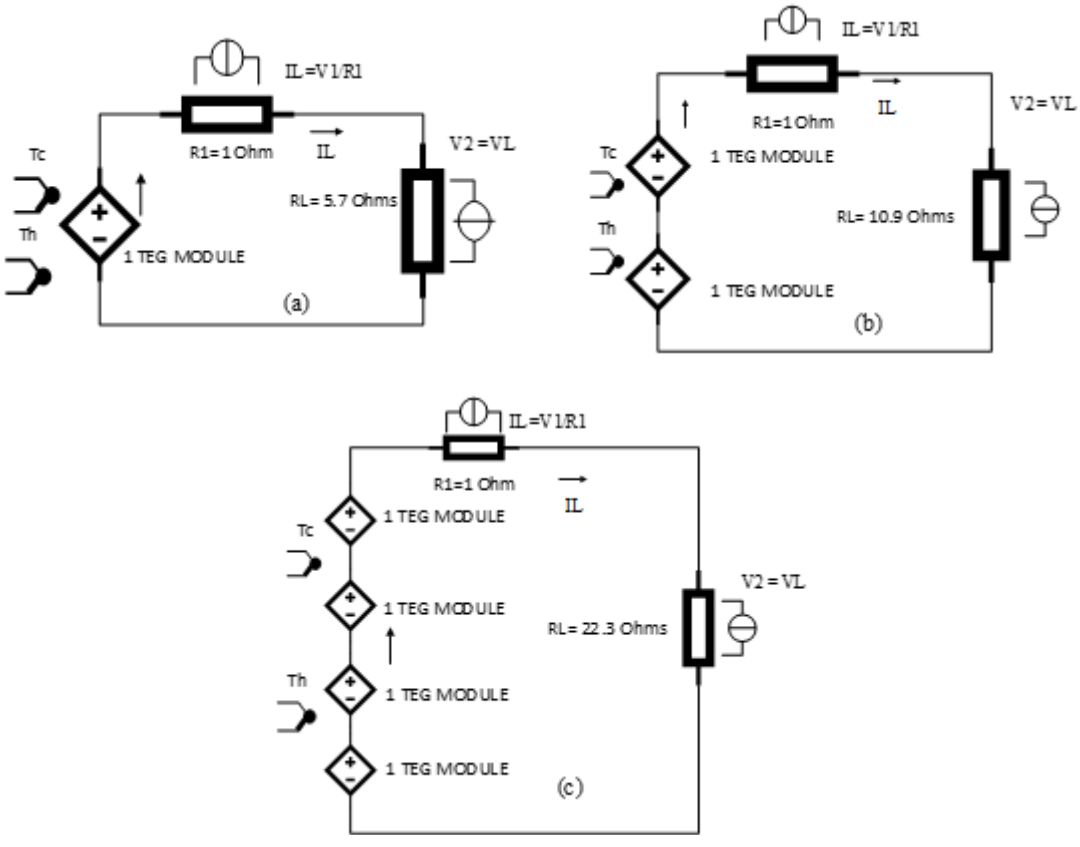

Fig. 8. Schematic representation of the electrical connection of the TEG Modules: a) One, b) Two, and c) Four TEG Modules.

In all the setups, the TEG internal resistance is matched to a pure resistive load and the only variable parameter was T_h whose values are extracted from the RAS site data at Nyalenda, Kisumu and varied from 22 ^{0}C to 69.2 ^{0}C. A graphite sheet with a thermal conductivity of 15.0 W/m.K is used to mitigate effects of temperature mismatch between the modules [19].

3.3 Field Trials Setup, System Design and Sizing

Based on the numerical and experimental findings, field trial setups are fabricated at the site to observe the practical behaviour of PV-TEG under ambient air and water-cooled conditions. The aquaculture system equipment ratings are used in the design and sizing of the PV-TEG hybrid system that is intended to supply power to the autonomus RAS.

3.3.1 Field Trials Setups

In the field trial setups, two 13 Wp PV modules are used. The first water cooled module with 10 TEG modules mounted on the back plate, while the second one was bare and used for open circuit voltage and temperature measurement. They were both subjected to the actual field weather conditions. The days were bright and irradiance is measured using a CMP-3 pyranometer and logged using a COMBILOG-1022 irradiance logger. PV and TEG temperatures are measured using K-type thermocouples and PV and TEG voltages logged using a KEYENCE NR-500 system. The same TEGs used in the laboratory setup are used in the field setup. Fig. 9 shows both the air-cooled and water-cooled setups while Fig. 10 schematically presents their respective electrical connection diagrams.

Fig. 9. Roof mounted air-cooled PV and water-cooled PV-TEG field setup

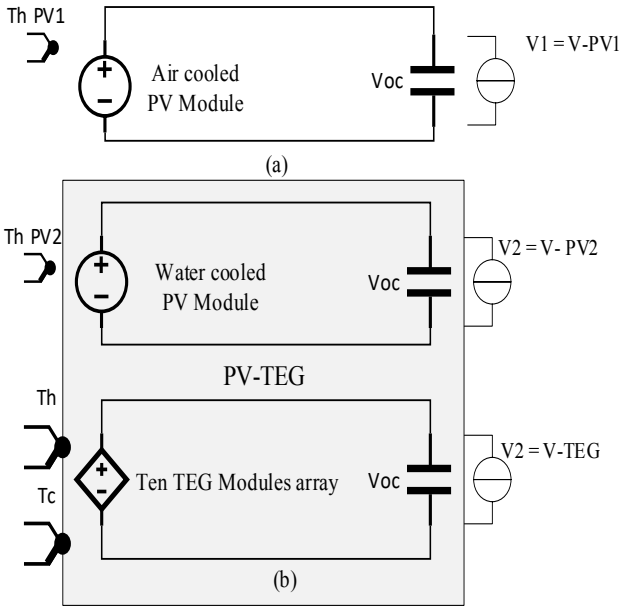

Fig. 10. Field setup electrical schematics (a) Air cooled PV (b) Water cooled PV-TEG

3.3.2 Field PV-TEG Power System Design

The PV-TEG system is intended to supply power to an autonomous Recirculating Aquaculture System in Nyalenda Kisumu. Using the weather data collected at the site over a one-year period, and from the Kenya solar potential database [35], the design is made to suit the daily load demand allowing three Days of Autonomy (DOA). The main power is supplied by the PV system with storage and the TEG complements the PV power. The load for the RAS consists of a Membrane Bio Reactor (MBR) and the ponds system as further presented in Table 3.

Table 3. The RAS electrical load

S/N	Load Description	Qty	Power (W)	Duty (Hr)	Energy (Wh)
1	MBR Pump	1	900	1	900
2	Filtrate pump	1	130	4.8	624
3	Blowers tank 1	1	215	2.5	537.5
4	Blowers tank 2	1	215	2.5	537.5
5	Sludge pump	1	40	1.5	60
6	Circulation pump	1	40	2	80
7	Sterilization	1	47	1	47
8	Ox guard control	8	20	24	3840
9	Bio filter pump	1	900	4	3600
10	Circulation pump	1	670	2	1340
11	UV-C generator	1	40	24	960
12	Filter pumps	1	1900	2.5	4750
13	H. tank pump	1	670	4	2680
14	RAS 1 blower	4	215	2	1720
15	RAS 2 blower	3	215	2	1290
16	Oxygen probes	1	20	24	480
17	Bio gas pump	1	450	3	1350
18	Computers	1	200	10	2000
19	Ox guard units	11	100	24	26400
20	Battery chargers	7	40	24	6720
21	24 V power unit	1	100	24	2400
	Total Load (Wh)				63216
	kWh				63.22

3.3.3 PV-TEG System Sizing Methodology

To get a complete and clear picture of the significance of the PV-TEG power generation system, the actual hybrid system is designed and sized factoring the demand and local conditions of the study site. The PV system is sized based on the average solar insolation for Nyalenda whose calculated 21-year daily average was 4.6 kWh [35]. The design parameters considered included; PV module type (polycrystalline) and size (275 W), battery storage type (L-ion) and size (48 V/50 Ah), system voltage (48 VDC), inverter type (pure sinewave), charge controllers (MPPT) and load profile and prioritization as presented in Table 3. The efficiencies of all the devices used are also taken into consideration.

The PV system output power is calculated as;

$$PV = \frac{daily\ load}{\eta_I \times \eta_B \times \eta_C \times \eta_{PV} \times PSH} \quad (14)$$

Where, η_I, η_C, η_B and η_{PV} are efficiencies of the inverter, charge controller, batteries and the PV modules, respectively, and PSH is Peak-sun hours for the site. The physical dimensions of the selected TEG and the surface area of the back plate of each PV module are used in the system design and sizing. The interfacing device between the TEG system and the battery bank, or the charge controller's resistance (impedance) is matched to the internal resistance of the TEG system.

The TEG power system is designed and sized considering mainly the field TEG hot side temperature, *Th* and the internal resistance of the entire TEG system. TEG modules are stuck on a honey comb cooling panel as shown in Fig. 11. Table 4 further presents the basic technical specifications for the selected TEG module in the design and sizing process.

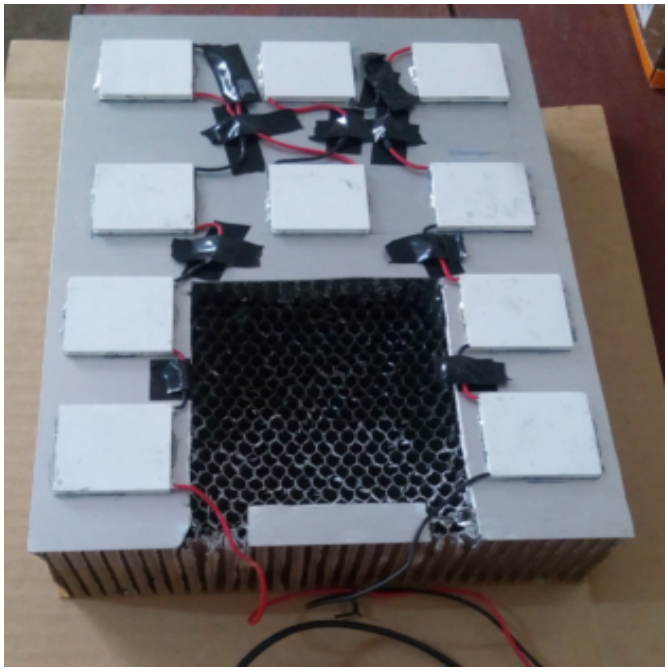

Fig. 11. TEGs stuck to the cooling panel

Table 4. TEG basic specifications

SP1848 -27145SA		
Δt - ^{0}C	Voc - Volts	I - mA
20 ^{0}C	0.97	225
40 ^{0}C	1.8	368
60 ^{0}C	2.4	469
80 ^{0}C	3.6	558
100 ^{0}C	4.8	669

Using the manufacturer's dimensions for the PV and TEG, the area of each PV back plate is 1.395 m^2 and that of each TEG module is 1.6 x 10^{-3} m^2. So, with a dead and edge space allowance of 30%, the back plate of each 275 Wp module would comfortably accommodate 600 TEGs.

4.0 Results and Discussion

4.1 Model Validation and Simulation Results

Simulation results from the developed model agree with the TEG theory and are validated with previous work done by Karami N. et al [33]. Fig. 12 presents a comparative analysis of the two studies. For the four parameters analysed, the trend is quite similar in both studies. The study by Karami N. et al however shows much lower values compared to the present study results because of the type of TEG used as they were not identical. The two TEG pellets differed in their internal parameters; Seebeck coefficients, electrical resistivities, length and thermal resistance that mostly affect the magnitude of their electrical outputs. The peak temperature used in the model was equivalent to the highest temperature achieved on site during field data collection so it was very different from the one used by Karami and his counterparts. Also, the accurate matching of the internal resistance and the load are factors that must have contributed to make the magnitudes vary because they affect the efficiency of the TEG. However, the sharp picks observed in the power and efficiency graphs, Figs. 12c and 12d, respectively, are due to the time period for the simulations. The behaviour of the TEGs however follow the same trend though the magnitude of the electrical outputs were different confirming the difference in samples used. From Figs. 12a and 12b, the voltage and current display higher values that rise gradually with time and temperature gradient to a high value of 0.75 V and the current peak of 0.14 mA. On the other hand, the TEG power rises to a peak of 20 mW and the efficiency rises to 11%. The observed values mostly depended on accurate matching of the simulation load resistance to the TEG internal resistance and the temperature gradient.

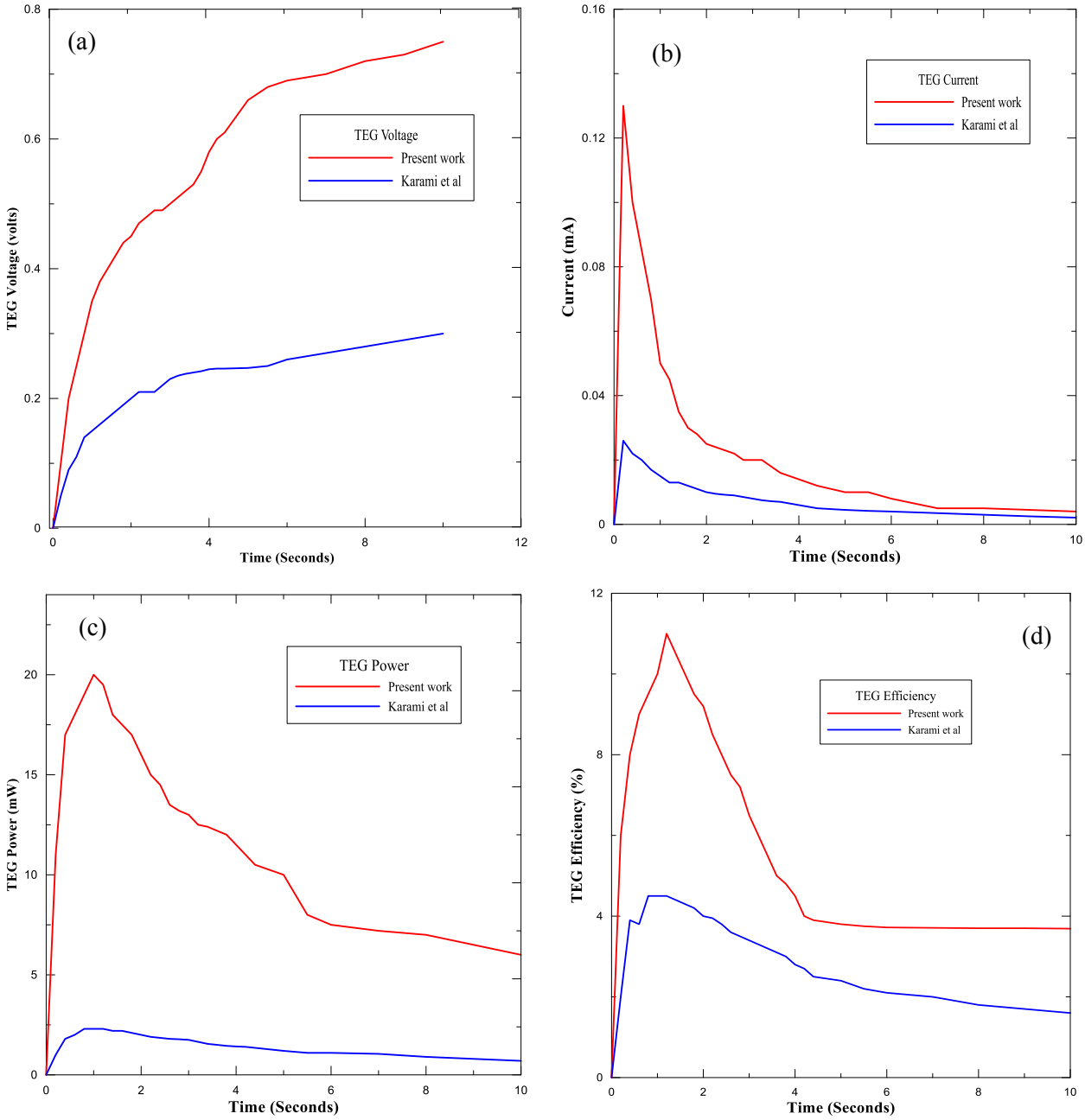

Fig. 12. Validation of present work; (a) Voltage, (b) Current, (c) Power and (d) Efficiency

4.2 Bench Setup Results

The bench setups in the laboratory succeeded the numerical simulations and results show that as T_h increases to the pre-set value of 69.2 ^{0}C and ΔT also increased, the TEG voltage increased to 0.6 V, 1.29 V and 2.41 V for one, two and four TEGs setups, respectively, as presented in Figs. 13a and 13b. The current had a negligible variance as expected due to series connection where the TEG maximum currents were 113.3 mA, 114.6 mA and 119 mA for the one, two and four TEGs, respectively, as presented in Figs. 13c and 13d. For one, two and four TEGs, the power increased to 73.98 mW, 134 mW and 287.39 mW as presented in Figs. 13e and 13f, respectively.

These results show that by carefully matching the TEG array internal resistance to the load or interface device resistance and connecting individual TEG modules in series, the output voltage can be scaled up increasing the power obtainable from the TEG modules. This is analogous to solar PV cells. Consequently, connecting such strings in parallel increases the current output. This therefore set the basis for the field trial setups.

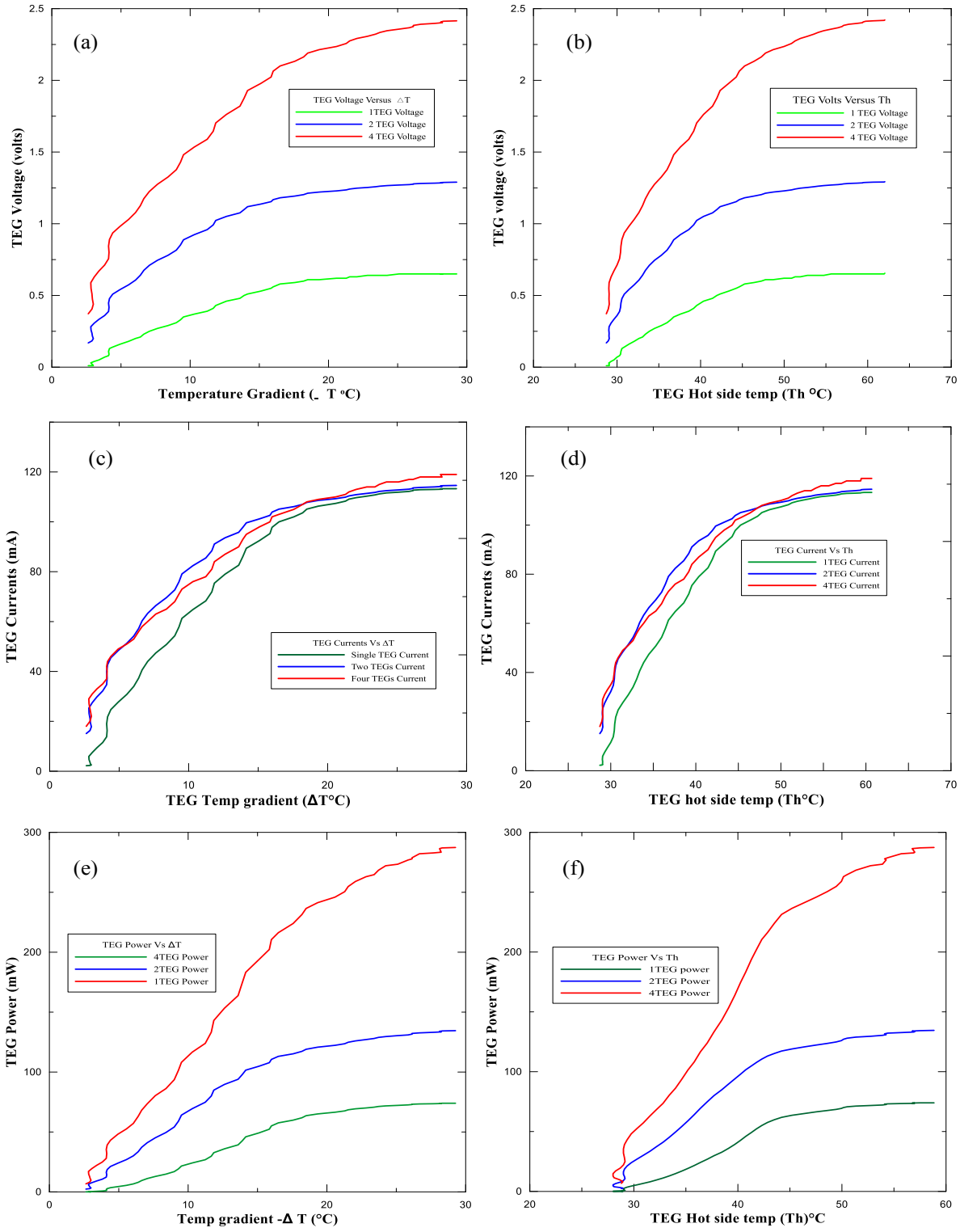

Fig. 13. TEG setups output measurements; (a) Voltages / ΔT, (b) Voltages / T_h, (c) Currents/ ΔT, (d) Currents / T_h, (e) Power / ΔT and (f) Power / T_h,

4.3 Field Trials and Final System Design Implications

The field PV-TEG trials were set up at the site in Nyalenda Kisumu where PV and TEG hot side temperature T_h of 62 ^{0}C and a maximum temperature gradient ΔT of 19.2 ^{0}C was achieved. During this test, PV and TEG average open circuit voltages of 20.35 V and 1.47 V, respectively, were obtained at an average irradiance of 920.01 W/m^2. Fig. 14 presents the variations of both the voltage and the temperature gradient with time. Both PV and TEG voltages were rather stable with PV voltages reducing slightly as temperature rose while that of the TEG increased slightly due to the increase in ΔT. The hot side temperature as well as the temperature gradient also

increased steadily with time reaching saturation after 30 seconds. Further, from the field trials, the obtained average temperature reduction between the air-cooled PV and water-cooled PV-TEG was 4.51 ^{0}C and the average electrical efficiency was 4.42% as presented in Fig. 15, and the peak temperature reduction and electrical efficiency are 8.45 ^{0}C and 13.75% respectively.

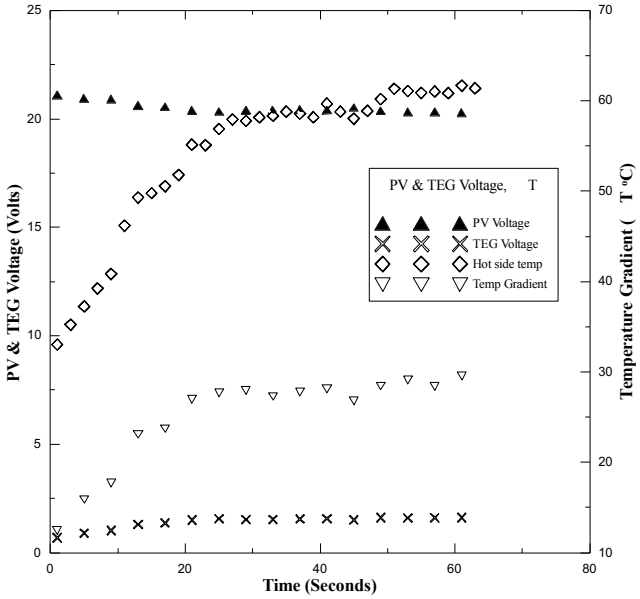

Fig. 14. PV-TEG field measurements

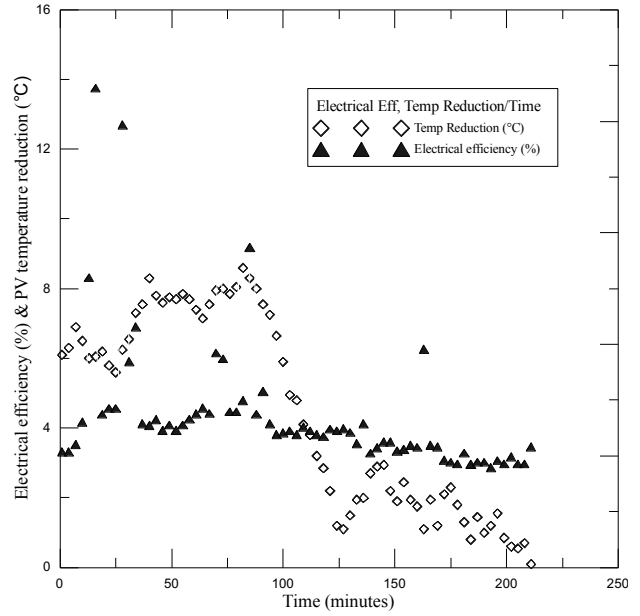

Fig. 15. PV electrical efficiency and temperature reduction

From the study investigations and using the daily energy requirements for the RAS as calculated in Table 3 to be 63.22 kWh and the site annual average irradiation of 4.6 kWh/m^2, a 19.13 kWp PV system is obtained which is equivalent to 20 kWp. The PV system will consist of 72 modules of 275 Wp each. One PV module will accommodate 600 TEG modules that will be capable of generating a peak power output of 43.7 W, so the total peak power from the TEG system is expected to be 3,146 W. The entire TEG system will be connected in a series-parallel formation to achieve a norminal voltage of the 48 V to charge the same battery bank as the PV. The TEG system directly contributes an additional 15.7% to the 20 kWp of the PV system power output. In addition, the PV system would generate 1.05% more power as compared to the original setup without cooling.

5.0 Conclusions

In this paper it has been shown both numerically and experimentally following a simulation approach that;

- When TEG modules' internal resistance is matched to the load impedance, maximum power output and efficiency of up to 9% can be obtained.
- When the PV system operating temperature is reduced by the TEG and cooling panels, about 1% of the PV power is gained.
- When TEG modules are stuck under PV modules especially in a tropical environment with PV temperatures ranging from 50 ^{0}C to 69.2 ^{0}C, up to 15% of the PV power can be generated by the TEG system array resulting in substantial additional amounts of power to the PV system.
- The performance efficiency of the PV system increases by 4.42% due to the cooling effect of the TEG with water on the cold side.

These results demonstrate that when TEGs are connected in a series and parallel formation and their internal resistance matched to the load, they can be relied on in generating considerable electrical power. Hence the PV+TEG power generation is highly attractive and promising with better efficiencies. The developed system can also be replicated in other sites with similar environmental conditions.

6.0 Acknowledgments

This work is supported by the European Union's Horizon 2020 research and innovation program under grant agreement No 689427.

7.0 References

[1] F. Creutzig, P. Agoston, J.C. Goldschmidt, G. Luderer, G. Nemet, R.C. Pietzcker, The underestimated potential of solar energy to mitigate climate change, Nature Energy. 2 (2017) 17140. doi:10.1038/nenergy.2017.140.

[2] A. Kane, V. Verma, Characterization of PV cell-environmental factors consideration, içinde: 2013 International Conference on Power, Energy and Control (ICPEC), IEEE, Sri Rangalatchum Dindigul, 2013: ss. 26-29. doi:10.1109/ICPEC.2013.6527618.

[3] A. Razak, Y.M. Irwan, W.Z. Leow, M. Irwanto, I. Safwati, M. Zhafarina, Investigation of the Effect Temperature on Photovoltaic (PV) Panel Output Performance, International Journal on Advanced Science, Engineering and Information Technology. 6 (2016) 682. doi:10.18517/ijaseit.6.5.938.

[4] Y. Xu, Y. X., L. Yang, Full-spectrum photon management of solar cell structures for photovoltaic–thermoelectric hybrid systems, Energy Conversion and Management. 103 (2015) 533-541. doi:10.1016/j.enconman.2015.07.007.

[5] N.K.Kasim, Hazim H.Hussain, Alaa N.Abed, Performance Analysis of Grid-Connected CIGS PV Solar System and Comparison with PVsyst Simulation Program, International Journal of Smart Grıd. Vol.3, (2019) 172-179.

[6] A.R. Nejad, A.R. Nejad, M.E. Abedi, A.R. Nejad, Production of electrical power in very extreme-temperature environmental conditions: A new implementation of thermoelectric generators, içinde: 2017 IEEE 6th International Conference on Renewable Energy Research and Applications (ICRERA), IEEE, San Diego, CA, 2017: ss. 468-472. doi:10.1109/ICRERA.2017.8191104.

[7] C. Temaneh-Nyah, L. Mukwekwe, An investigation on the effect of operating temperature on power output of the photovoltaic system at University of Namibia Faculty of Engineering and I.T campus, içinde: 2015 Third International Conference on Digital Information, Networking, and Wireless Communications (DINWC), IEEE, Moscow, Russia, 2015: ss. 22-29. doi:10.1109/DINWC.2015.7054211.

[8] C.U. Ike, effects of temperature on performance of a solar PV system in E. Nigeria, International Journal of Engineering And Science. Vol.3 (2013) 10-14.

[9] M. Benhmida, C. Hajjaj, R. Bendaoud, H. Amiry, S. Bounouar, A. Ghennioui, F. Chanaa, S. Yadir, A. Elhassnaoui, H. Ezzaki, A PVT Cooling System Design and Realization: Temperature Effect on the PV Module Performance Under Real Operating Conditions, International Journal Of Renewable Energy Research. Vol.9 (2019).

[10] H.A. Hussien, M. Hasanuzzaman, A.H. Noman, A.R. Abdulmunem, Enhance Photovoltaic/Thermal System Performance by Using Nanofluid, (2013) 5.

[11] N. Yadav, M. Gupta, K. Sudhakar, Energy assessment of floating photovoltaic system, içinde: 2016 International Conference on Electrical Power and Energy Systems (ICEPES), IEEE, Bhopal, India, 2016: ss. 264-269. doi:10.1109/ICEPES.2016.7915941.

[12] F. Kawtharani, M. Hammoud, A. Hallal, A. Shaito, A. Assi, I. Assi, Cooling P.V Modules using phase change materials, içinde: 2017 29th International conference on microelectronics (ICM), IEEE, Beitut, Lebanon, 2017. doi:10.1109/ICM.2017.8268830.

[13] I. Al Siyabi, S. Khanna, S. Sundaram, T. Mallick, Experimental and Numerical Thermal Analysis of Multi-Layered Microchannel Heat Sink for Concentrating Photovoltaic Application, Energies. 12 (2018) 122. doi:10.3390/en12010122.

[14] W.A.M. Al-Shohani, R. Al-Dadah, S. Mahmoud, Reducing the thermal load of a photovoltaic module through an optical water filter, Applied Thermal Engineering. 109 (2016) 475-486. doi:10.1016/j.applthermaleng.2016.08.107.

[15] M. Rosa-Clot, P. Rosa-Clot, G.M. Tina, C. Ventura, Experimental photovoltaic-thermal Power Plants based on TESPI panel, Solar Energy. 133 (2016) 305-314. doi:10.1016/j.solener.2016.03.024.

[16] G. Li, X. Chen, Y. Jin, Analysis of the Primary Constraint Conditions of an Efficient Photovoltaic-Thermoelectric Hybrid System, (2017) 12.

[17] B.S Dallan, J. Schumann, F. Lesage, Performance evaluation of a photoelectric–thermoelectric cogeneration hybrid system, Solar Energy. 118 (2015) 276-285.

[18] A. Belkaid, I. Colak, K. Kayisli, R. Bayindir, H.I. Bulbul, Maximum Power Extraction from a Photovoltaic Panel and a Thermoelectric Generator Constituting a Hybrid Electrical Generation System, içinde: 2018 International Conference on Smart Grid (icSmartGrid), IEEE, Nagasaki, Japan, 2018: ss. 276-282. doi:10.1109/ISGWCP.2018.8634534.

[19] K. Li, C. Liu, P. Chen, A 1 KW Thermoelectric Generator for Low-temperature Geothermal Resources, içinde: Thirty-Ninth Workshop on Geothermal Reservoir Engineering, Stanford University, Stanford, California, 2014: s. 12.

[20] G. Li, S. Shittu, T.M.O. Diallo, M. Yu, X. Zhao, J. Ji, A review of solar photovoltaic-thermoelectric hybrid system for electricity generation, Energy. 158 (2018) 41-58. doi:10.1016/j.energy.2018.06.021.

[21] S. Soltani, A. Kasaeian, H. Sarrafha, D. Wen, An experimental investigation of a hybrid photovoltaic/thermoelectric system with nanofluid application, Solar Energy. 155 (2017) 1033-1043. doi:10.1016/j.solener.2017.06.069.

[22] J. Lin, T. Liao, B. Lin, Performance analysis and load matching of a photovoltaic–thermoelectric hybrid system, Energy Conversion and Management. 105 (2015) 891-899. doi:10.1016/j.enconman.2015.08.054.

[23] J. Zhang, H. Zhai, Z. Wu, Y. Wang, H. Xie, M. Zhang, Enhanced performance of photovoltaic–thermoelectric coupling devices with thermal interface materials, Energy Reports. 6 (2020) 116-122. doi:10.1016/j.egyr.2019.12.001.

[24] T.M. Abu-Rahmeh, Efficiency of Photovoltaic Modules Using Different Cooling Methods: A Comparative Study, Journal of Power and Energy Engineering. 05 (2017) 32-45. doi:10.4236/jpee.2017.59003.

[25] H. Hashim, J.J. Bomphrey, G. Min, Model for geometry optimisation of thermoelectric devices in a hybrid PV/TE system, Renewable Energy. 87 (2016) 458-463. doi:10.1016/j.renene.2015.10.029.

[26] K. Kawabuchi, T. Yachi, Analysis of the heat transfer characteristics in a thermoelectric conversion device, içinde: 2012 International Conference on Renewable Energy Research and Applications (ICRERA), IEEE, Nagasaki, Japan, 2012: ss. 1-5. doi:10.1109/ICRERA.2012.6477265.

[27] B. Asfandiyar, B. Cai., L.-D. Zhao., J.-F. Li., High thermoelectric figure of merit ZT > 1 in SnS polycrystals, Journal of Materiomics. 6 (2020) 77-85. doi:10.1016/j.jmat.2019.12.003.

[28] A. Hidaka, T. Tsuji, S. Matsumoto, A thermoelectric power generation system with ultra low input voltage boost converter with maximum power point tracking, içinde: 2012 International Conference on Renewable Energy Research and Applications (ICRERA), IEEE, Nagasaki, Japan, 2012: ss. 1-5. doi:10.1109/ICRERA.2012.6477474.

[29] R.B. Kolambekar, K. Bhole, Development of Prototype for Waste Heat Energy Recovery from Thermoelectric System at Godrej Vikhroli Plant, (2015) 6.
[30] D. Rowe, Thermoelectrics and environmentally friendly sources of electrical energy, içinde: Thermoelectrics and environmentally friendly sources of electrical energy, 1999: ss. 1251-1256.
[31] E. Kanimba, Z. Tian, Modeling of a Thermoelectric Generator Device, içinde: S. Skipidarov, M. Nikitin (Ed.), Thermoelectrics for Power Generation - A Look at Trends in the Technology, InTech, 2016. doi:10.5772/65741.
[32] Z.M. Dalala, Energy harvesting using thermoelectric generators, içinde: 2016 IEEE International Energy Conference (ENERGYCON), IEEE, Leuven, Belgium, 2016: ss. 1-6. doi:10.1109/ENERGYCON.2016.7514088.
[33] N. Karami and N. Moubayed, New Modeling Approach and Validation of a Thermoelectric Generator, IEEE. (2014).
[34] M.J. Dousti, A. Petraglia, M. Pedram, Accurate Electrothermal Modeling of Thermoelectric Generators, içinde: 2015: ss. 1603-1606.
[35] H. Gichungi, Solar Potential in Kenya, (2012). https://www.sv.uio.no/iss/english/research/projects/solar-transitions/announcements/Kenya-Henry_Gichungi.pdf.